Impingement of an Electron-Bombardment Ion Rocket," TN D-1657, 1963, NASA.

[12] King, H. J. et al., "Low Voltage 30-Cm Ion Thruster," NASA CR-120919, Feb. 1972, Hughes Research Labs., Malibu, Calif.

[13] Macie, T. W. et al., "Integration of a Flight Prototype Power Conditioner with a 20-Cm Ion Thruster," AIAA Paper 71-159, New York, 1971.

[14] Byers, D. C., "An Experimental Investigation of a High-Voltage Electron-Bombardment Ion Thruster," *Journal of the Electrochemical Society*, Vol. 116, No. 1, Jan. 1969, pp. 9–17.

[15] Bechtel, R. T., "Discharge Chamber Optimization of the SERT II Thruster," *Journal of Spacecraft and Rockets*, Vol. 5, No. 7, July 1968, pp. 795–800.

[16] Lathem, W. C. and Adam, W. B., "Theoretical Analysis of a Grid-Translation Beam Deflection System for a 30-Cm Diameter Kaufman Thruster," TM X-67911, 1971, NASA.

JANUARY 1973 J. SPACECRAFT VOL. 10, NO. 1

# Ion Thruster Thermal Characteristics and Performance

L. WEN,* J. D. CROTTY,† AND E. V. PAWLIK‡
*Jet Propulsion Laboratory, Pasadena, Calif.*

**Experimental and analytical results for a typical 20-cm-diam, hollow-cathode ion thruster are reported. The foundation of the investigation was the application of thermal model correction techniques. Pertinent thermal properties and plasma heating characteristics of the thruster were determined through correlation and integration of temperature measurement data with a single-state Wiener-Kalman filter. The thruster self-heating levels on various parts were realistically estimated. Analytically predicted temperatures were forced to agree with the measured values for the purpose of constructing a corrected thermal model, which could then be used to evaluate more realistic thruster circumstances and environments. The expected accuracy of the resultant analytical network model was demonstrated to be ±10 K. Thruster thermal performance data for a typical five-thruster array are presented as functions of environmental solar intensities. The thermal analyses are also extended to a 30-cm thruster system.**

## Nomenclature

$A$ = thermal radiation surface area, cm$^2$
$b_{jk}$ = the $(j, k)$th element of the matrix $[\mathbf{B} + \mathbf{HPH}^T]^{-1}$
$\mathbf{C}$ = a diagonal matrix with elements $c_k^2$
$c_k$ = uncertainty limit of parameter $v_k$
$\mathbf{D}$ = a diagonal matrix with elements $(\Delta T_m)^2$
$\mathbf{E}$ = covariance matrix of vector $\mathbf{R}$
$e_m$ = expected random error in measurement $m$
$\mathscr{F}_{ij}$ = Hottel's script-$F$ factor
$\hat{F}_{ij}$ = total radiation exchange factor, $\hat{F}_{ij} = \mathscr{F}_{ij}/\varepsilon_i\varepsilon_j$
$H$ = a $M \times L$ matrix of sensitivity coefficients, $\partial T_i/\partial v_k$
$K_{ij}$ = thermal conductance between nodes $i$ and $j$
$L$ = number of parameters to be determined
$M$ = number of measurements
$\mathbf{P}$ = covariance matrix of vector $\mathbf{X}$
$Q$ = net thermal energy input to node $i$
$\mathbf{R}$ = residual vector with elements $r_1, r_2, \ldots, r_m$
$r_m$ = observation residual
$s_k$ = the $(k, k)$th element of matrix $\mathbf{P}$
$T$ = nodal equilibrium temperature
$\Delta T$ = deviation between measured data and calculated results
$v$ = parameter to be determined
$\Delta v$ = correction factor
$\mathbf{X}$ = a $L$-vector consisting of all correction factors
$\mathbf{Y}$ = a $M$-vector with elements $\Delta T_m$
$\varepsilon$ = total hemispherical emittance
$\sigma$ = Stefan Boltzmann constant

*Subscripts and superscripts*

$i$ = nodal value
$j$ = integer
$k$ = integer, parameter count
$m$ = integer, measurement count
$c$ = integer, measurement count
$c$ = calculated value
$*$ = measured value
$\circ$ = nominal value
$T$ = transpose of matrix

Received May 30, 1972; revision received September 18, 1972. This paper presents the results of one phase of research carried out at the Jet Propulsion Laboratory, California Institute of Technology, under Contract NAS 7-100, sponsored by NASA. The authors acknowledge the assistance of the Electric Propulsion Applications Laboratory staff of the Jet Propulsion Laboratory. The contributions to the instrumentation and test setups by E. Hopper were invaluable in obtaining the thruster temperatures.

Index categories: Electric and Advanced Space Propulsion; Thermal Modeling and Experimental Thermal Simulation.

* Senior Engineer. Member AIAA.
† Consultant.
‡ Member Technical Staff. Member AIAA.

## Introduction

THE integration of a thruster array with a spacecraft requires a comprehensive understanding of their thermal interaction under various operating conditions. Some basic thruster thermal constraints include: 1) maintenance of vaporizer control at high temperatures; 2) prevention of freezing of the mercury propellant; 3) maintenance of cathode temperature in the proper range; and 4) maintenance of thruster housing temperatures below a limiting temperature to prevent overheating of magnets. Accurate thermal analysis is required in all stages of spacecraft development. It serves as a useful tool in evaluating thruster design configurations[1,2] and in predicting over-all spacecraft system performance.

The reliability of thermal analytical results is governed by the parameters describing the mathematical model. Detailed information about the following parameters has to be available prior to any meaningful thermal analysis of ion thrusters: 1) thermophysical properties of thruster components, such as thermal contact conductances, surface emittances, and material thermal conductivities; 2) thruster self-heating pattern due to electron, ion, and plasma radiation heating; 3) design configurations and arrangement of clustered arrays; and 4) environmental conditions, solar heating levels, and the thermal coupling between the thruster array and the spacecraft.

Because of the complexity of the design and the operating mode, accurate information on the self-heating distribution and

the thruster thermal properties is usually unavailable. The uncertainties involved in such parameters play a critical role in the accuracy of the thermal analysis. A realistic thermal model cannot be constructed without first establishing close estimations of these parameters. In the present investigation, major emphasis was placed on the determination of the thermal properties of thruster components and on the self-heating distribution under various operating modes. Analytically predicted temperatures based on a preliminary mathematical model were compared with measured values as forcing functions for model corrections. Once a reliable analytical model was constructed, predictions of thruster thermal performance under specified conditions could be carried out in a straightforward manner.

## Basic Thruster Configuration and Experimental Apparatus

Experimental studies to provide the required temperature data were performed with a 20-cm-diam electron-bombardment ion thruster that utilizes a hollow cathode as the electron source and mercury as the propellant. Thrusters of this type have been used in the Solar Electric Propulsion System Tests (SEPST) studies, some results of which are presented in Ref. 3. The basic configuration of the thruster design is similar to that described in Ref. 4, with modifications made at the cathode, the pole piece, and the feedline system in order to accommodate a high-voltage isolator similar to the unit described in Ref. 5.

The nominal operating level for this thruster is 1000–2000 w of throttleable output power (0.5–1.0 amp of ion beam current at a net accelerating voltage of 2000 v). Other parameters are: arc voltage, 35 v; accelerator voltage, $-1000$ v; and propellant utilization, 90%. The experiments were carried out in a vacuum chamber with a diameter of 0.914 m and a length of 2.13 m maintained at a pressure of $2.66 \times 10^{-4}$ to $10.64 \times 10^{-4}$ N/m$^2$ ($2 \times 10^{-6}$ to $8 \times 10^{-6}$ torr).

For this investigation, a thermal network model was constructed to represent the thruster. Thirty-eight thermocouples were installed on various components. Their locations are shown in Fig. 1. Fourteen independent thermal tests were performed to calibrate the thermal network. The thruster was heated externally by electrical heating at the cathode, isolator, and vaporizer. The data obtained were used to determine the thermophysical properties of the network, for which the total heat input and its distribution were well-specified. After the thermal parameters were established, thirteen experiments were performed with plasma discharges. Thruster component temperature data measured at various operating conditions were applied to determine the self-heating distribution. Each experiment was repeated at least once to ensure the accuracy of the measurements. Most temperature measurements were reproduced within $\pm 5$°K.

## Analytical Network and Parameter Adjustments

Based on the design configuration, a lumped mass thermal network model consisting of 96 nodes was constructed. The basic nodal energy balance relationship for each node of the system is of the following form:

$$Q_i - \sum_{j=1}^{96} K_{ij}(T_i - T_j) - A_i\varepsilon_i\sigma T_i^4 + \varepsilon_i \sum_{j=1}^{96} \varepsilon_j A_j \hat{F}_{ij}\sigma T_j^4 = 0 \quad (1)$$

For the first 14 experiments, the heating level (electrical heating) and boundary conditions were specified. The set of 96 nonlinear nodal energy equations can be solved simultaneously for the temperature distribution, $T_1, T_2, \ldots, T_{96}$, in terms of all of the thermophysical properties, $v_k$, which include all conductances $K_{ij}$ and surface emittances $\varepsilon_i$.

$$T_i = T_i(v_k), \qquad k = 1, \ldots, L \quad (2)$$

The exact value of the thermal parameters were not available. A set of a priori estimates with associated uncertainty limits

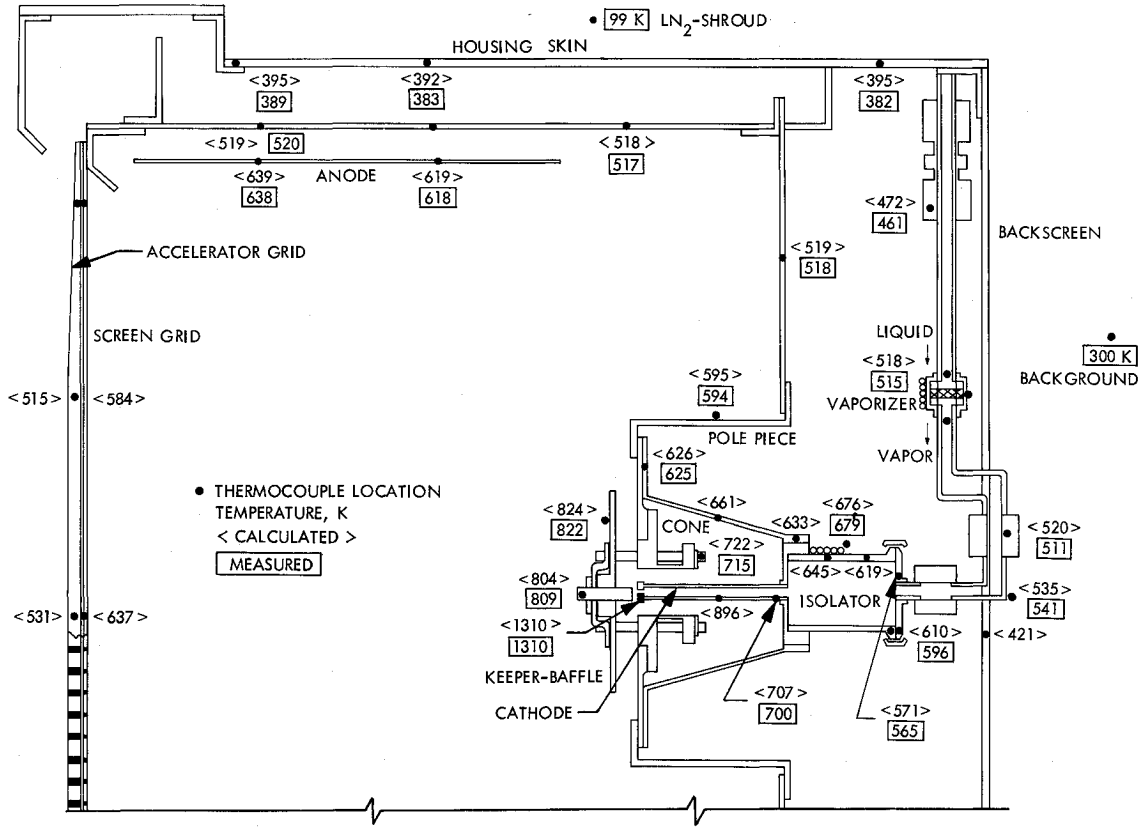


**Fig. 1 Temperature distribution of a 20-cm thruster operating at full output power.**

could be assumed as $v_k^0 \pm c_k$, according to the surface and material specifications. Applying such a priori guesses on all parameters, one could numerically evaluate the thermal model, using the thermal analyzer program "HEAT"[6] to yield a preliminary temperature distribution $T_i^0$ with corresponding sensitivity coefficients $\partial T_i/\partial v_k$.

Because of inaccurate parameter values assumed in the model, the preliminary temperature distribution may not be in good agreement with actual measured data. The application of thermal model correction techniques to update and correct an analytical network has been a subject of study by many investigators.[7-9] The basic philosophy lies in the utilization of temperature measurement data to adjust the thermophysical parameters involved in the model such that accurate temperature predictions can be expected from the corrected model. A statistical estimation scheme based on the single-stage Wiener-Kalman filtering technique is presently under development at the Jet Propulsion Laboratory. This particular filtering scheme was selected to perform the parameter adjustment procedure, based primarily on the following consideration: 1) the estimation scheme is weighted by the a priori information to yield a minimum-variance estimator; 2) the scheme is capable of yielding a set of optimal estimates for under-determined systems—i.e., systems where the number of unknown parameters is greater than the number of measurements; 3) the corrected model offers good agreement between the measured data and the analytical results.

The algorithm of the estimation scheme is briefly stated as follows: Consider a system with $M$ measured temperatures and $L$ parameters. For each measurement the experimental data, $T_m^*$, can be related to the preliminary calculation, $T_m^0$, and the correction factors through a first-order Taylor series

$$T_m^* = T_m^0 + \sum_{k=1}^{L} (\partial T_m/\partial v_k) \cdot \Delta v_k + r_m \tag{3}$$

In matrix notation, this relationship may be expressed as

$$\mathbf{Y} = \mathbf{HX} + \mathbf{R} \tag{4}$$

or

$$\begin{bmatrix} T_1^* - T_1^\circ \\ \vdots \\ T_M^* - T_M^\circ \end{bmatrix} = \begin{bmatrix} \frac{\partial T_1}{\partial v_1} & \frac{\partial T_1}{\partial v_2} & \cdots & \frac{\partial T_1}{\partial v_L} \\ \vdots & \vdots & \cdots & \vdots \\ \frac{\partial T_M}{\partial v_1} & \frac{\partial T_M}{\partial v_2} & \cdots & \frac{\partial T_M}{\partial v_L} \end{bmatrix} \begin{bmatrix} \Delta v_1 \\ \vdots \\ \Delta v_L \end{bmatrix} + \begin{bmatrix} r_1 \\ \vdots \\ r_M \end{bmatrix} \tag{5}$$

In order to apply the Wiener-Kalman filtering scheme, certain statistical characteristics of the observed quantities have to be established. The a priori covariance $\mathbf{P}$ of the parameter vector was calculated according to the following relationship:

$$\mathbf{P} = [\mathbf{H}^T\mathbf{D}^{-1}\mathbf{H} + \mathbf{C}^{-1}]^{-1}$$

The covariance matrix of the residual vector $\mathbf{R}$ is represented by a diagonal $M \times M$ matrix $\mathbf{E}$

$$\mathbf{E} = \begin{bmatrix} e_1^2 & & 0 \\ & \ddots & \\ 0 & & e_M^2 \end{bmatrix} \tag{6}$$

According to the Wiener-Kalman scheme, the optimal estimation of the correction factor $\mathbf{X}$ can be computed from the following matrix equation:

$$\hat{\mathbf{X}} = \mathbf{PH}^T[\mathbf{E} + \mathbf{HPH}^T]^{-1}\mathbf{Y} \tag{7}$$

The working formula for evaluating the correction factor is

$$\Delta v_k = s_k \sum_{i=1}^{M} \sum_{j=1}^{M} (\partial T_i/\partial v_k) b_{jk} (\Delta T_j)$$

Because of the large number of thermal parameters involved in the model, the thruster system was first partitioned into three subsystems for parameter determination before the final network was put together. The final analytical model was capable or reproducing measured temperature distributions with satisfactory accuracy. The temperature deviations between the calculated and measured results are within $\pm 10°$K for most system components.

It should be noted that the view factor between internal thruster components and grids were not treated as parameters and, therefore, were not subjected to model corrections. They were determined through extensive efforts prior to the application of the statistical estimation scheme. Introducing the view factors as adjustable parameters would require modification of the present technique to accommodate additional constraints. (For example, the sum of all view factors for each node must equal unity.) Future studies are anticipated which will upgrade the capability of the estimation technique toward incorporating constraint relations. Such a procedure should enhance the accuracy of the analysis and greatly reduce the time spent in view-factor computations. Also, imposing a power constraint relation on the estimation scheme could guarantee that the sum of the self-heating power distributions would always equal the known total applied power.

## Thruster Self-Heating Distribution

During operation, thruster self-heating is caused by electron and ion bombardment, as well as radiation and electron heating. The self-heating pattern has been observed by many investigators[1,10] as a complex function of the design configuration, the operating conditions (beam current, arc current, etc.), and the discharge mode.

A priori estimates of the heat delivered to various components of the thruster were required to initiate and guide the statistical estimation process. These estimates were arrived at by using the plasma properties of a similar thruster functioning near the same operating conditions.[10] By using the ion-flux and plasma-potential distributions, the ion bombardment and surface recombination heating could be estimated. Electron heating at the node and keeper electrodes was calculated as the current to these components multiplied by the work function of the surface. Heating due to the kinetic energy of the electrons was scaled directly from Masek's work.[10] Power to heat the cathode was estimated using the results of Ref. 11. Power lost to the ion beam was estimated as the beam current multiplied by the ionization potential of mercury in addition to plasma radiation losses.

After the above heating mechanisms had been determined, there remained a difference between these calculated heating powers and the measured arc power. It amounted to approximately 35% of the power delivered to the arc chamber. This was assumed to be the amount of power lost by radiation from the plasma. It was further assumed that this power loss would be distributed to each portion of the thruster in direct proportion to its exposed area. The fraction lost to the ion beam can therefore be determined by using the open area of the acceleration grid. Estimates were made for the two operating points that represent the nominal operating range for the thruster (0.5- and 1.0-amp beam current). All estimates are listed in Table 1 along with the resulting thruster temperatures for these assumed power levels.

The Wiener-Kalman scheme was applied again to obtain an optimal estimation of the self-heating distribution at the two levels of beam current that were examined. The estimates determined in the above fashion were used as the a priori guesses in the adjustment process, and the corrected network based on the thermal test was utilized to minimize the uncertainty involved in the thermal parameters.

The initial guesses and the final results together with the corresponding temperatures are presented in Table 1. Measured temperature data are also listed for comparison.

High-voltage arcing problems on the thermocouple leads imbedded on the grids forced a reduction to a net accelerating

**Table 1 Self-heating power distributions**

| Thruster component | $T_m$, °K | A priori value: Power, w | A priori value: Uncertainty, % | A priori value: $T_c$, °K | A priori value: $T_m - T_c$, °K | Final value: Power, w | Final value: $T_c$, °K | Final value: $T_m - T_c$, °K |
|---|---|---|---|---|---|---|---|---|
| | Currents: | | Ion beam, 0.500 amp<br>Arc, 3.7 amp (35.2 v) | | Keeper, 0.8 amp (5.1 v)<br>Accelerator, 0.0015 amp (2600 v) | | | |
| Keeper-baffle | 707 | 8.0 | 50 | 661 | 46 | 11.2 | 702 | 5 |
| Pole piece | 545 | 9.6 | 20 | 528 | 17 | 9.9 | 545 | 0 |
| Cathode tip | 1212 | 10.0 | 50 | 1104 | 108 | 12.6 | 1204 | 8 |
| Pole piece (side) | 515 | 10.2 | 30 | 501 | 14 | 14.0 | 514 | 1 |
| Rear plate | 459 | 20.4 | 30 | 455 | 4 | 16.1 | 460 | −1 |
| Anode (screen) | 562 | 23.0 | 20 | 551 | 11 | 28.1 | 563 | −1 |
| Anode (aft) | 540 | 19.1 | 20 | 543 | −3 | 14.7 | 541 | −1 |
| Housing | 461 | 12.6 | 40 | 454 | 7 | 13.1 | 462 | −1 |
| Screen grid | 555 | 8.6 | 20 | 543 | 12 | 5.9 | 556 | −1 |
| Accelerator grid | 471 | 6.2 | 30 | 447 | 24 | 10.1 | 470 | 1 |
| | Currents: | | Ion beam, 1.000 amp<br>Arc, 7.1 amp (35.2 v) | | Keeper, 0.8 amp (3.3 v)<br>Accelerator, 0.0028 amp (2600 v) | | | |
| Keeper-baffle | 822 | 12.9 | 50 | 755 | 63 | 20.6 | 824 | −2 |
| Pole piece | 665 | 16.7 | 20 | 625 | 56 | 18.2 | 626 | −1 |
| Cathode tip | 1310 | 14.0 | 50 | 1265 | 45 | 15.4 | 1310 | 0 |
| Pole piece (side) | 594 | 18.6 | 30 | 575 | 15 | 31.1 | 595 | −1 |
| Rear plate | 518 | 39.2 | 30 | 517 | 1 | 36.7 | 519 | −1 |
| Anode (screen) | 639 | 44.0 | 20 | 641 | −2 | 44.2 | 640 | −1 |
| Anode (aft) | 618 | 36.5 | 20 | 630 | −12 | 28.8 | 619 | −1 |
| Housing | 517 | 20.9 | 40 | 519 | −2 | 20.2 | 518 | −1 |
| Screen grid | 636[a] | 16.2 | 20 | 645 | −9 | 11.6 | 637 | −1 |
| Accelerator grid | 530[a] | 11.1 | 30 | 519 | 11 | 11.8 | 531 | −1 |

[a] Temperature data extrapolated from Ref. 2.

voltage of 1600 v. This was not expected to seriously affect the results. Thermocouples on the screen grid accelerator grid were eventually burned out at high-beam current conditions. Temperature data used for determining power distribution on the grids for the 1.0-amp conditions were extrapolated from related experimental work.[2] These data are also included in Table 1.

A closer match of the calculated and measured results could be obtained, if desired, by further iterations. However, since the results already agreed to within the accuracy of the thermocouple measurements, further iterations would be superfluous.

## Thermal Performance

Once the thermophysical properties of the thruster and the self-heating power distribution were established by the statistical correction scheme, the finalized thermal model could be applied to yield reliable analytical results for thruster thermal performance as a function of environmental heating and also for operation in an array. Transient thermal behavior under thruster startup conditions could also be analyzed in the same fashion, provided that transient temperature data were available. In the present study, sample analyses were made for a 20-cm thruster operating at full output power under steady-state conditions. The operating conditions used were as follows: beam current = 1 amp; arc current = 7.1 amp; arc voltage = 35.2 v; keeper current = 0.8 amp; keeper voltage = 3.3 v; power voltage = 3.3 v; power in magnets = 3.3 w; accelerator power = 7.2 w. The corresponding self-heating power distribution was listed in Table 1.

### Temperature Comparisons

Single-thruster operating temperatures are compared to analytical predictions for the operating conditions specified above. The predicted component temperatures are compared to thermocouple measurements only at steady-state levels. The experiment was performed in a liquid-nitrogen-cooled vacuum chamber maintained at 98°K and $8.84 \times 10^{-4}$ N/m$^2$ ($6.65 \times 10^{-6}$ torr). Ten temperature values were utilized to complete the self-heating power distribution. This power distribution was then utilized to compute the temperature profile of the entire thruster. Most temperature deviations between the measured data and the analytical results were within ±10°K, as shown in Fig. 1.

### Effects of Environmental Heating on Single-Thruster Performance

During a typical mission, the expected solar environment could vary considerably. Environmental heating from solar illumination are infrared radiation from other proximate bodies affects the thruster skin temperature, which effectively determines the internal temperature distribution. In the present study, it is assumed that the thruster back is facing the spacecraft, which is maintained at 300°K. Under the operating conditions specified previously, the relationship between the effective environmental heating and the mean thruster housing temperature can be analyzed parametrically. Figure 2 illustrates the energy balance relationship as a function of mean thruster skin temperature.

In the absence of any environmental heating ($Q_E = 0$), the thruster side wall is heated solely from the thruster interior, and all the net heating received will be reradiated to space ($Q_W = Q_1$). As the environmental heating level increases ($Q_E > 0$), the skin temperature also increases, and the amount of internal power dissipated through the wall, $Q_1$, decreases. The energy radiated from the side wall of the thruster to space always remains the sum of the internal contribution, $Q_1$, and environmental heating, $Q_E$: $Q_W = Q_1 + Q_E$. Total thermal energy generated internally, $Q_I$, which includes self-heating power and all electrical heating, is dissipated through the wall, $Q_1$; the front grids, $Q_3$; and the back screen, $Q_2$ (to the spacecraft maintained at 300°K). The relationship $Q_I = Q_1 + Q_2 + Q_3$ remains true until excessive environmental heating raises the mean skin temperature above 575°K. The direction of heat flow

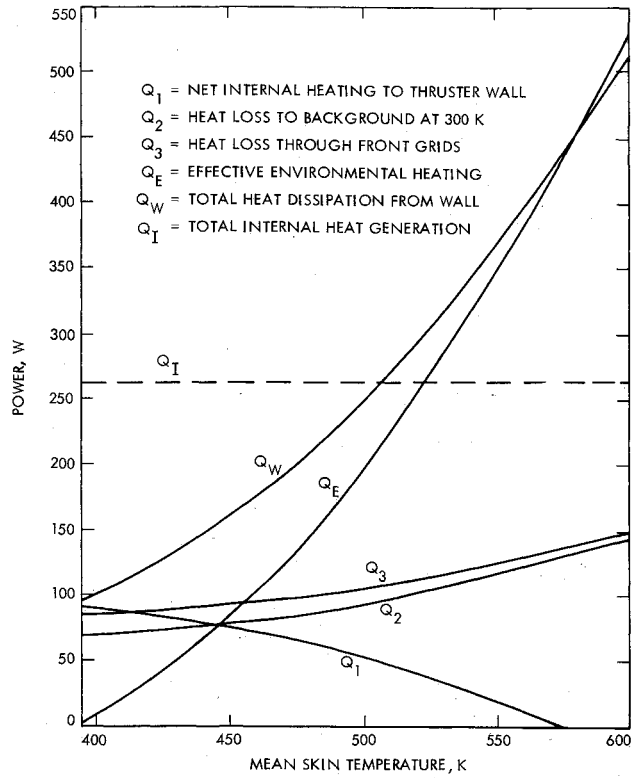


**Fig. 2 Energy balance relationship.**

between the thruster interior and the wall, $Q_1$, is reversed, which implies that additional net heating of the amount $Q_E - Q_W$ will be added to the thruster interior and will have to be dissipated through the front grids and the back screen.

As the thruster skin temperature changes, the internal temperature distribution will be affected. In Fig. 3, the effect of mean skin temperature on the steady-state temperatures of the anode, screen grid, accelerator grid, and keeper were shown. The rear part of the anode is approximately 15°K cooler than the front part, whose temperature is shown in the figure.

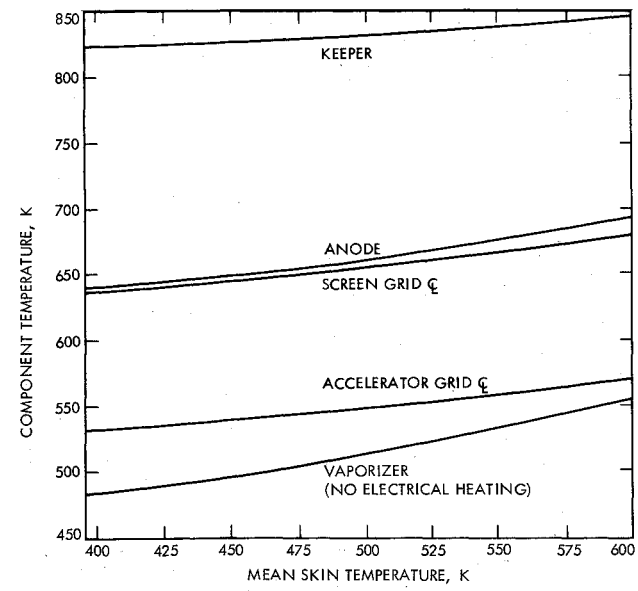


**Fig. 3 Thruster component temperature variation resulting from environmental heating.**

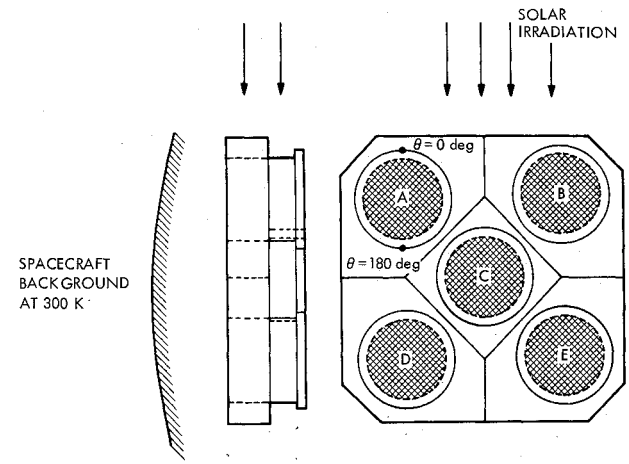


**Fig. 4 Geometrical configuration of a five-thruster clustered array.**

### Effects of Solar Environment on Clustered Array

In one proposed mission design,[1,2] ion thrusters were arranged in a clustered array. Figure 4 illustrates the geometrical arrangement of a five-thruster array and the aluminum supporting structure (assumed to be 3.25 mm thick for heat conduction consideration). Structure and thruster skin temperatures were calculated for a solar environment ranging from zero- to five-sun irradiances (700 mw/cm$^2$). The analytical results for the averaged thruster skin temperatures are shown in Fig. 5 under the assumption that: 1) all five thrusters are identical and operated at the same conditions; 2) the back side of the array is completely shaded by the spacecraft at 300°K; and 3) the ratio of solar absorptance and infrared emittance of all external bare metal surfaces is unity. At the no-sun condition, the mean

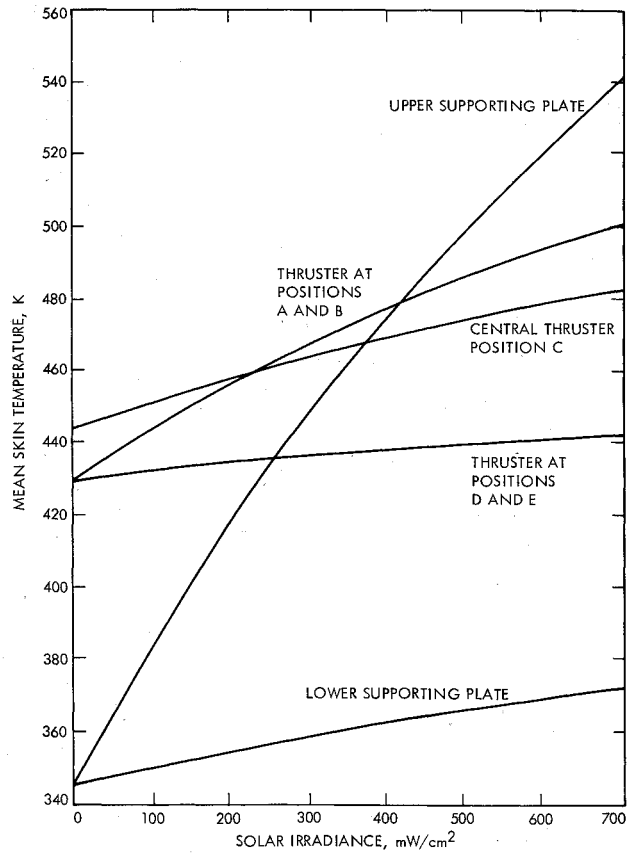


**Fig. 5 Effect of solar heating on a 20-cm thruster wall in a five-thruster array.**

skin temperature of the central thruster (position C in Fig. 5) is about 15°K higher than that of the thrusters in the top row (positions A and B) and bottom row (positions D and E). At the five-sun condition, the top row thrusters are approximately 50°K warmer than the shaded ones (bottom row). The back portion of the thruster body (shaded by the structure) has a skin temperature approximately 10°K higher than the average skin temperature of the front portion, which has a circumferential gradient of 30°K between positions having solar angles of 0° and 180°.

#### Vaporizer Controllability

The gaseous mercury flow rate from the vaporizer to the cathode is controlled by an electrical heater maintaining the vaporizer at a designated temperature. If thermal perturbations, such as a varying solar environment, exist that cause this temperature to be maintained or exceeded without electrically supplied power, then a loss of control would result. In order to maintain the operating conditions specified above, the vaporizer temperature was held at 520°K. The electrical power required to maintain this vaporizer set temperature is plotted in Fig. 6 for the clustered array operating at solar irradiances between 0 and 700 mw/cm$^2$. It is observed that the controllability becomes marginal with 700-mw/cm$^2$ solar illumination. Excessive environmental heating would require negative electrical heating (cooling) to maintain the controllability, and a different thermal design of the thruster would be needed to accommodate such situations.

It is also crucial to the thruster operation that the feedline be maintained above 233°K to keep the liquid mercury from freezing and possibly penetrating the vaporizer. A far-sun (2.5-a.u.) operating situation was examined. Thrusters at positions A and E were considered to be in operation, while thrusters B, C, and D were standby.

The thruster located at position D would have a mean skin temperature of 243°K, as compared to 415°K at position A (in operation). Without any electrical heating, the feedline system in thruster D is maintained at 265°K when the back of the array is shaded completely by the spacecraft at 300°K. However, if the thruster back screen surface is completely exposed to space (0°K), it would require approximately 0.25-w electrical heating at the vaporizer heater to maintain the feedline system at 233°K.

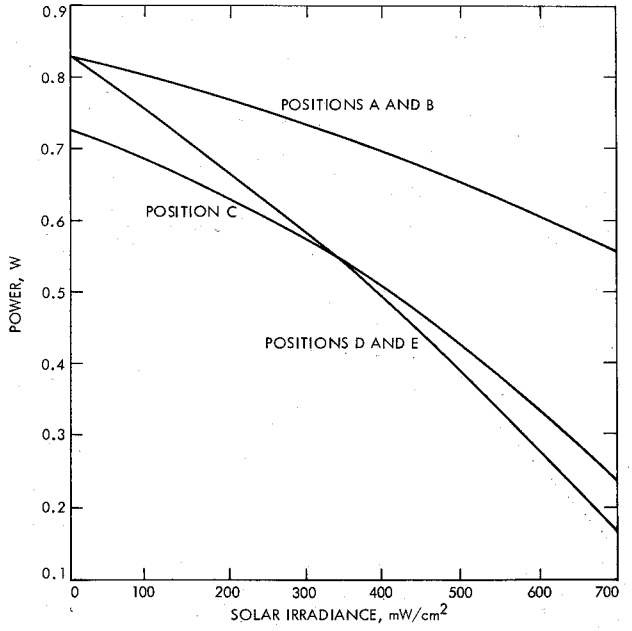


**Fig. 6 Electrical power required for vaporizer control.**

## Thruster Dimension Effects

For high-power missions (15 kw or higher), a thruster size in the 30-cm range appeared to be most appealing.[1,2] An attempt was made to extend the thermal performance analysis in a preliminary fashion for the large-size thrusters of interest. Since sufficient experimental data for the 30-cm thruster operation was lacking, the analysis was made based on the following assumptions: 1) The geometrical configuration of the 30-cm thruster clustered array is proportional to the 20-cm one, except for the feedline system, which remained unchanged. 2) The 30-cm thruster was assumed to be operated at a beam current of 2 amp, and the arc-chamber losses were assumed to remain the same as those for the smaller thruster; i.e., the losses measured in eV/ion would be the same. Based on this assumption, the self-heating power distribution of a 30-cm thruster operating at a 2-amp beam current would have twice the value of the heating level of a 20-cm thruster operating at a 1-amp beam current. In the analysis the self-heating power distribution was taken to be twice the value reported in Table 1, except for the cathode power, which was assumed to be 15 w. Under the assumed operating conditions, the thermal performance of the 30-cm thruster array was analyzed in the same fashion as that for the 20-cm system. The back surface of the thruster array is radiatively coupled with the spacecraft, which is assumed to be maintained at 300°K. Figure 7 illustrates the steady-state temperature levels of various thruster components for a 30-cm thruster located at position A or B in the clustered array.

## Summary of Results

The reliability of the statistical estimation scheme depends upon the measured data and the measurement accuracy. If the number of experimental data points equals the number of variables to be determined, a deterministic mathematical system and thus a set of unique solutions could be obtained. In general practice, however, the number of variables usually exceeds the number of experimental data points. For such under-determined systems, conventional mathematical methods

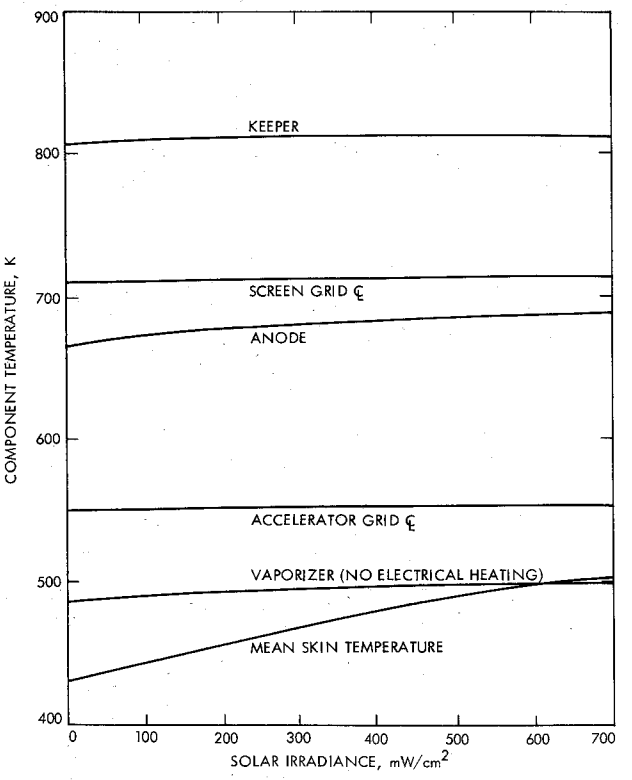


**Fig. 7 Effect of solar heating on a 30-cm thruster positioned at the upper row of a five-thruster array.**

cannot be applied. Statistical estimation schemes must be utilized to yield an optimal estimation of parameters by taking both the experimental data and the a priori information into consideration. The reliability of the estimation increases with the amount of data available.

In the present investigation, the number of temperature measurements was considered to be sufficient to lead to reliable results. Each experiment was repeated at least once to insure the measurement accuracy. Most temperature measurements were reproducible within $\pm 5°K$.

Detailed temperature measurements in conjunction with a corrected thermal network model of the thruster allow a realistic description of thruster thermal performance. The applicability of the statistical estimation technique has been demonstrated to be a useful tool for constructing reliable thermal models, for analyzing ion thrusters, and for determining thermal interactions between the thruster array and the spacecraft. Based on the results presented in this investigation, it was concluded that: 1) A realistic thermal model can be constructed to represent the thruster with an expected accuracy of $\pm 10°K$. 2) The power extracted from the plasma can be estimated from experiments and used for further studies of the thruster plasma processes. Heat losses from the plasma to various parts of the thruster can be determined, allowing thruster inefficiencies to be examined. 3) Analytical techniques can be effectively applied in thruster design to predict component temperature variations as functions of array configuration and solar environment. These techniques could be extended to include the analysis of thruster startup conditions. 4) The thermal interaction and power dissipation relationship between the thruster array and the spacecraft can be analyzed for realistic design configurations and can be utilized to obtain a set of design parameters for the thruster to accommodate all design temperature constraints imposed on both the thruster array and the spacecraft.

## References

[1] Bayless, J. R. et al. "LM Cathode Thruster System," Final Report Supplement, Contract JPL 952131, Sept. 1970, Hughes Research Lab., Malibu, Calif.

[2] Seliger, R. et al. "Ion Engine Thruster Vector Study," Final Report, Contract JPL 952129, March 1970, Hughes Research Lab., Malibu, Calif.

[3] Masek, T. D., "Solar Electric Propulsion Breadboard Thruster Subsystem Test Results," AIAA Paper 72-507, Bethesda, Md., 1972.

[4] Pawlik, E. V., "Performance of a 20-cm-Diameter Electron-Bombardment Hollow-Cathode Ion Thruster," TM 33-468, Feb. 15, 1971, Jet Propulsion Lab., Pasadena, Calif.

[5] King, H. J. and Poeschel, R. L., "30-cm Diameter, Low Specific Impulse, Hollow Cathode Mercury Thruster," AIAA Paper 70-1099, Stanford, Calif., 1970.

[6] Beckman, W. A., "HEAT (Heat Transfer Computer Program in Fortran V Language)," EES Report 37, July 1972, Engineering Experiment Station, Univ. of Wisconsin, Madison, Wis.

[7] Ishimoto, T. and Pan, H. M., "Thermal Network Correction Techniques," AIAA Paper 70-821, Los Angeles, Calif., 1970.

[8] Toussaint, M., "Verification of the Thermal Mathematical Model for Artificial Satellites: A New Test Philosophy," *AIAA Progress in Astronautics and Aeronautics: Thermophysics of Spacecraft and Planetary Bodies*, Vol. 20, edited by G. B. Heller, Academic Press, New York, 1967, pp. 611–629.

[9] Howell, J. R., "The Effect of Data Uncertainties on Thermal Analysis," AIAA Paper 72-60, San Diego, Calif., 1972.

[10] Masek, T. D., "Plasma Properties and Performance of Mercury Ion Thrusters," TR 32-1483, June 15, 1970, Jet Propulsion Lab., Pasadena, Calif.

[11] Goldstein, R., Pawlik, E. V., and Wen, L., "Preliminary Investigations of Ion Thruster Cathodes," TR 32-1536, Aug. 1, 1970, Jet Propulsion Lab., Pasadena, Calif.

[12] "Solar Electric Multi-Mission Spacecraft (SEMMS), Phase A Final Report Technical Summary," Document 617-4, March 1972, Jet Propulsion Lab., Pasadena, Calif. (internal document).